REPORT DOCUMENTATION PAGE

Form Approved
OMB No. 0704-0188

1. REPORT DATE *(DD-MM-YYYY)*
May 14, 2008

2. REPORT TYPE
Final Performance Report

3. DATES COVERED *(From – To)*
Jan 2007 – Dec 2007

4. TITLE AND SUBTITLE
Final Performance Report

Demonstration and Modeling of Material Responses Achieved Through Contradirectional Coupling

5a. CONTRACT NUMBER

5b. GRANT NUMBER
FA9550-07-1-0029

5c. PROGRAM ELEMENT NUMBER

6. AUTHOR(S)
Anthony Grbic

5d. PROJECT NUMBER

5e. TASK NUMBER

5f. WORK UNIT NUMBER

7. PERFORMING ORGANIZATION NAME(S) AND ADDRESS(ES)

Dept. of Electrical Eng. and
Computer Science
University of Michigan
1301 Beal Ave., 3244 EECS
Ann Arbor, MI, 48109-2122

8. PERFORMING ORGANIZATION REPORT NUMBER

9. SPONSORING / MONITORING AGENCY NAME(S) AND ADDRESS(ES)
Air Force Office of
Scientific Research
875 North Randolph St.
Arlington, VA 22203

10. SPONSOR/MONITOR'S ACRONYM(S)
AFOSR

11. SPONSOR/MONITOR'S REPORT NUMBER(S)

12. DISTRIBUTION / AVAILABILITY STATEMENT

DISTRIBUTION STATEMENT A: UNLIMITED

13. SUPPLEMENTARY NOTES

14. ABSTRACT
This report describes the development of broadband and reduced-loss negative permeability and negative refractive index metamaterials at microwave frequencies. The reported structures exhibit fractional bandwidths that are greater than 40%. Simulation and experimental results are described which confirm the electromagnetic properties of the proposed structures. Analytical modeling of the proposed structures is also discussed.

15. SUBJECT TERMS
metamaterials, negative refractive index, transmission lines, periodic structures, coupling

16. SECURITY CLASSIFICATION OF: a. REPORT	b. ABSTRACT	c. THIS PAGE	17. LIMITATION OF ABSTRACT	18. NUMBER OF PAGES	19a. NAME OF RESPONSIBLE PERSON
			UU	18	Anthony Grbic
					19b. TELEPHONE NUMBER *(include area code)* 734-647-1797

FINAL PERFORMANCE REPORT
FA9550-07-1-0029
Demonstration and Modeling of Material Responses Achieved Through Contradirectional Coupling

Anthony Grbic
Assistant Professor
Dept. of Electrical Engineering and Computer Science
University of Michigan
1301 Beal Avenue, 3244 EECS
Ann Arbor MI, 48109-2122
agrbic@umich.edu

OBJECTIVES

The objective of the three year effort was to investigate various material responses that can be achieved through contradirectional coupling between electromagnetic backward-waves (waves with antiparallel phase and group velocities) and forward-waves (waves with parallel phase and group velocities). In the first year of this effort, there was an emphasis on achieving broadband negative permeability and broad negative refractive index (NRI) volumetric structures through such coupling mechanisms. This work will be continued and various other material responses will be investigated as part of an AFOSR Young Investigator Award (FA9550-08-1-0067), which replaces the present grant.

STATUS OF EFFORT

The first goal of this research was to develop metamaterials that exhibit a negative permeability response over a broad bandwidth (fractional bandwidth >40%) of operation, both in simulation and experiment. Preliminary work by the PI showed that certain metamaterial topologies that rely on contradirectional coupling between a forward free-space wave and a backward-wave guided by a transmission line can exhibit negative permeability over fractional bandwidths that exceeds 40% [1,2]. The proposed volumetric negative permeability structures were designed with the aid of analytical models and the refined through full-wave simulation. Following the design stage, a prototype negative permeability structure was fabricated and tested [3]. Transmission experiments were conducted on the prototype to determine its electromagnetic properties and negative permeability bandwidth. The prototype exhibited a fractional bandwidth in excess of 40% [4].

The second goal of this effort was to combine the broadband negative permeability structure with an array of wires, which exhibits a negative permittivity, to produce a broadband NRI medium. The NRI medium was designed and tested to experimentally verify its properties and NRI (backward-wave) bandwidth of 44.3% [3,4].

Finally, analytical models of the proposed structures were developed [3,5]. The operation of the negative permeability medium was explained through multiconductor transmission-line analysis. The analysis provided an intuitive explanation of the proposed structures' operation and revealed the underlying physics. The analytical work showed how contradirectional coupling occurs and what effect each design parameter has on the structure's performance.

RESULTS

The PI's research group developed a volumetric metamaterial (shown in Figure 1) that exhibits a negative permeability over bandwidths in excess of 40%

[1,2,3,4]. Conventional negative permeability metamaterials consisting of split-ring resonators (SRRs) typically exhibit bandwidths of only 10% [6,7]. Therefore, this new metamaterial represents a significant improvement over prior art.

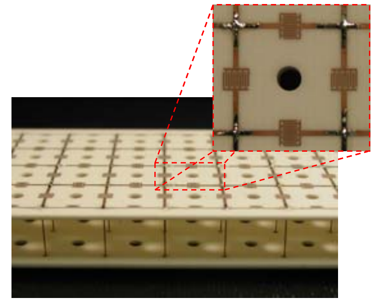

Figure 1: A practical implementation of a broadband negative permeability metamaterial at microwave frequencies.

The broad negative permeability bandwidth of the structure shown in Figure 1 has been verified both in simulation and experiment by the PI's research group [3,4]. Figure 2 shows its simulated dispersion curve. As can be seen from the curve, the structure exhibits a wide stopband. The stopband results from the fact that the permeability remains negative over a wide range of frequencies while the permittivity remains positive. Since the permeability and permittivity of the structure have opposite signs, waves cannot propagate trhoughout this frequency range and a stopband forms. These simulation results therefore support the claim that the structure exhibits a wide negative permeability.

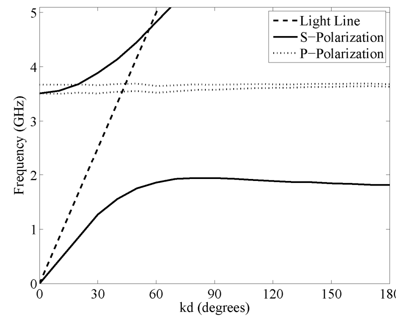

Figure 2 Simulated dispersion curve of the negative permeability metamaterial shown in Figure 1. S-polarization is the polarization of interest.

The stopband (negative permeability bandwidth) shown in Figure 2 was confirmed experimentally by conducting transmission measurements through the four-cell slab of the negative permeability metamaterial shown in Figure 1 [3,4]. These experiments, which confirm the simulated results presented in [1,2], were performed by the PI's research group. In the experiments, transmission measurements between two coaxially-fed probes, placed 7cm from either face of the slab, were performed. The transmission coefficient through the four-cell slab is plotted as a function of frequency in Figure 3. The figure shows that the structure exhibits very high attenuation in the region where the simulated dispersion curve of Figure 2 predicts a stopband. The plot shows an attenuation of greater than 20dB for the four-cell slab when compared to the case when there is no slab present. These experimental results provide strong evidence that the structure shown in Figure 1 exhibits a broadband negative permeability, given that the structure's response is primarily magnetic.

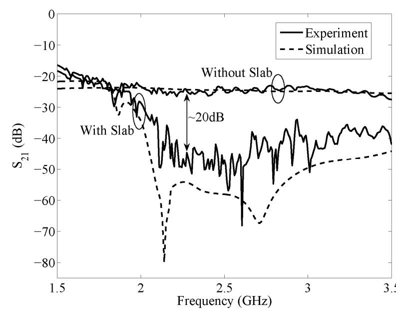

Figure 3: Stopband performance of the negative permeability slab shown in Figure 1. Measurements are denoted by the solid line and simulated results are shown with the dashed line. The relatively flat lines indicate the transmission without the negative permeability slab present.

Adding a vertical wire to the negative permeability structure shown in Figure 1 (in order to achieve negative permittivity) lead to a volumetric structure that exhibits a negative refractive index (NRI) over an extremely wide bandwidth. The resulting NRI structure is shown in Figure 4. The simulated dispersion curve for this NRI structure (shown in Figure 5) indicates that it exhibits a negative-refractive-index bandwidth of 44.3%, ranging from 1.83GHz to 2.86GHz. This is more than triple the bandwidth of previously reported volumetric NRI structures [6,7]. Therefore, this new metamaterial constitutes a major improvement over the state of the art.

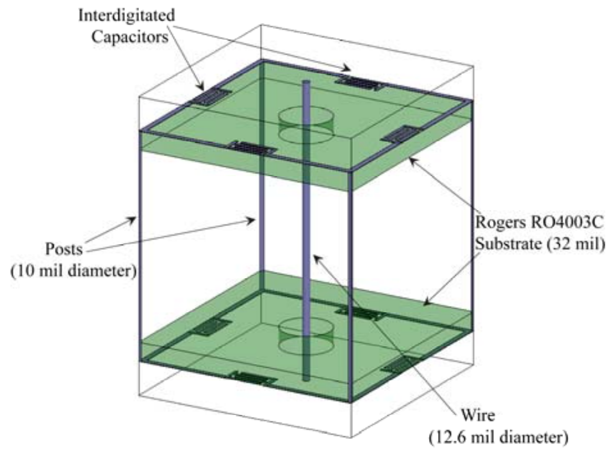

Figure 4: A metamaterial that exhibits an extremely wide negative- refractive-index (backward-wave) bandwidth at microwave frequencies.

Not only does the structure exhibit a much wider bandwidth than previously reported structures, but it also exhibits a greatly improved loss performance. As was claimed in the initial proposal, the increased bandwidth improves the structure's loss performance by pushing the high-loss resonances of the structure further from its operating frequencies. To show how much lower the losses are for the proposed structure (see Figure 4) over exisiting NRI structures, the PI's research group tackled the most restrictive of applications: superlensing. Despite the years of effort in metamaterials to demonstrate superlensing using a slab of volumetric negative refractive index material, such experiments have eluded research groups. The main stumbling block has been loss. It is well known that the resolution of a negative refractive index slab is highly dependent on its loss performance [8,9,10]:

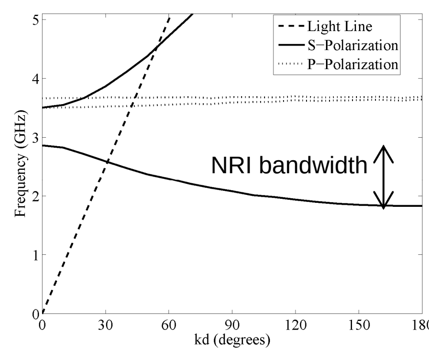

Figure 5: Simulated dispersion curve for the negative refractive index (NRI) structure shown in Figure 4. These simulated results show that the structure exhibits a negative refractive index bandwidth of 44.3 %. S polarization is the polarization of interest.

In our experiments, we imaged a dipole antenna to subwavelength resolutions using a NRI slab composed of unit cells shown in Figure 4 [4]. Figure 6 plots the measured electric field amplitude along the focal plane of the NRI slab, as well as the diffraction-limited curve as a reference. A comparison of the diffraction-limited curve and the experimental plot clearly shows that the proposed slab design does achieve super-resolution. The half-power beamwidth of the diffraction-limited curve is 0.36 wavelengths, as is expected for an S-polarized line source. The half-power beamwidth of the experimental curve is 0.252 wavelengths, which corresponds to a resolution enhancement of 2.0. In other words, the negative index lens has a resolution two times better than that of a conventional lens.

Due to the reduced losses, subwavelength focusing using a volumetric negative refractive index metamaterial slab was achieved for the first time using the developed NRI medium. These results have been submitted to the IEEE Transactions on Antennas and Propagation in July of 2007. The manuscript [4] is still under review and has been attached as an appendix.

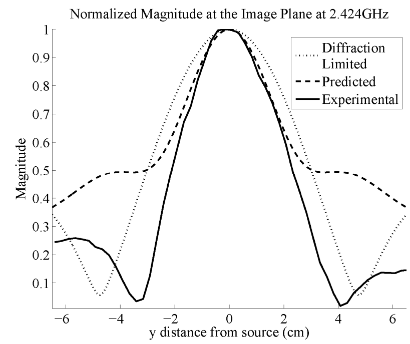

Figure 6: Normalized electric field magnitude at the focal (image) plane of a NRI slab. The experimental electric field magnitude is plotted with a solid line, the theoretical diffraction-limited pattern is plotted with a dotted line. Simulation results are shown with a dashed line.

The negative permeability and NRI experiments discussed in this section were conducted in an oversized parallel plate waveguide. Future work includes free-space measurement of the material parameters of the developed volumetric negative permeability and NRI structures as well as free-space superlensing experiments. This effort will be part of the AFOSR Young Investigator Award (FA9550-08-1-0067) the PI was awarded for the years 2008-2011.

ACCOMPLISHMENTS

Bandwidth Improvement:

As was mentioned in the previous section, the bandwidth of conventional NRI metamaterials employing wires and split-ring resonators (SRRs) is about 10% [6,7]. In the structures proposed by the PI (see Figure 4), this bandwidth is significantly increased by coupling the individual resonators together through direct electrical connections [2]. Figure 5 shows the negative index bandwidth of the structure fabricated by the PI’s research group [3,4]. The upper and lower cutoff frequencies for the negative refractive index region are 2.86GHz and 1.83GHz, respectively. The resulting NRI (backward-wave) bandwidth of 44.3% is more than three times larger than that of conventional SRR/wire NRI structures [6].

Loss Reduction

The losses in conventional NRI metamaterials, such as the split-ring resonator/wire medium are inherently high, since their frequency of operation is very close to the resonant frequency of the split-ring resonators, where the medium transitions from positive permeability to negative permeability [11]. By increasing the NRI (backward-wave) bandwidth, the operating frequency is shifted away from this resonance. Consequently, the losses at the operating frequency are lower for the broadband structures developed by the PI. Figure 7 shows the simulated loss performance of the structure depicted in Figure 4. At the operating frequency of 2.45 GHz (where the refractive index of the structure is equal to -1), the losses for an entire four-cell slab are only 0.37dB [4].

In order to compare the losses for slabs of different lengths, the losses can be quantified using a parameter called the Figure of Merit (FOM) [12]. It is given by the equation $FOM = \left|\frac{n'}{n''}\right|$, where n' and n'' are the real and imaginary parts of the index of refraction, respectively. In [13], the FOM was found to be 3.1 at 14.7 GHz. In [14], the FOM was calculated to be 12 at 3.74 GHz, and the authors of the paper claimed this FOM to be the highest value reported to date. However, the broadband NRI medium designed by the PI's research group had a FOM of 47.9 at 2.45 GHz, nearly four times that of the highest previously-reported FOM for volumetric materials. This FOM was also comparable to planar transmission-line NRI implementations. The FOM for the planar NRI transmission-line medium that the PI developed during his Ph.D. studies [15] was 32.1 at 1 GHz.

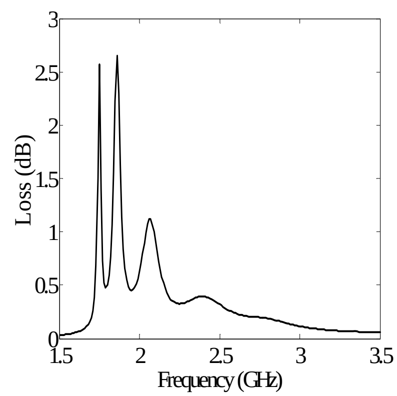

Figure 7: Transmission losses for a four-cell NRI slab consisting of unit cells shown in Figure 4.

It should be noted that the frequencies of operation of the volumetric NRI media presented in [13,14] are higher than those of the NRI medium designed by the PI's research group. This increase in frequency, however, does not account for the difference in reported FOM values. To confirm this, the PI's research group has recently designed a high frequency version of the broadband NRI medium shown in Figure 4 that operates at 10 GHz. In simulation, the new structure still exhibits a high figure of merit (FOM=40), demonstrating that low-loss NRI metamaterials can be achieved even at higher (X-band) frequencies. The PI's research group is currently fabricating the structure and will test it during the summer of 2008.

Analytical Modeling

The broadband NRI medium developed in this work has been successfully modeled using multiconductor transmission-line analysis [3,5]. This simplified analysis provides closed form expressions for the resonant points of the structure, which can be used for design purposes. The PI and his graduate student are currently writing a journal paper on the subject.

IMPACT OF THIS WORK

The developed broadband negative permeability medium could find applications in diverse areas of electrical engineering. The structure exhibits an electromagnetic stopband over a wide frequency range which will find applications in antenna and filter design. Further, the development of the broadband negative permeability medium has enabled the development of broadband and low loss NRI materials.

At microwave frequencies, the proposed NRI metamaterials have far-reaching applications ranging from imaging to communications. From such materials, volumetric superlenses could be constructed that have the potential for resolutions well beyond the diffraction limit. In 2004, a planar 2D superlens was developed by the PI that overcomes the diffraction limit[16]. This lens was planar and focusing was restricted to guided microwaves on a printed circuit board. The experimental results put to rest any objections to Pendry's superlens concept, but the planar implementation of the lens had limited application. This sponsored work has developed volumetric implementations of such lenses that can be interfaced to free space, thereby broadening their application.

Benefits of this technology include improved wireless sensors, conformal and compact far-field lenses for communications[17], reflectionless lenses and radomes, novel couplers, antenna designs[18], and beam steering technology. Improvements in NRI materials such as those demonstrated in this work could also lead to higher resolution microwave probing systems[19].

PERSONNEL SUPPORTED

Anthony Grbic, Assistant Professor – two months summer salary

PUBLICATIONS:

<u>Journal Papers:</u>

S. M. Rudolph and A. Grbic, "A Volumetric Negative- Refractive-Index Medium Exhibiting Broadband Negative Permeability," *Journal of Applied Physics*, **102**, 013904, July 2007.

S.M. Rudolph, A. Grbic, “Super-Resolution Focusing Using Broadband, Volumetric NRI Media,” *IEEE Trans. on Antennas and Propagation*, under review, submitted July 2007.

Refereed Conference Papers:

A. Grbic, “A 2-D Composite Medium Exhibiting Broadband Negative Permittivity and Permeability," in *IEEE Antennas and Propagation Society International Symposium*, pp. 4133-4136, Albuquerque, NM, July 9-14 2006.

S. M. Rudolph and A. Grbic, “A Printed Circuit Implementation of a Broadband Volumetric Negative-Refractive-Index Medium," *IEEE Antennas and Propagation Society International Symposium*, pp. 2542-2545, Honolulu, HI, June 9-15 2007.

S.M. Rudolph, A. Grbic, “Modeling of Volumetric Negative-Refractive-Index Media Using Multiconductor Transmission-Line Analysis, *Applied Computational Electromagnetics Society Conference (ACES)*, 4 pages, Niagara Falls Canada, March 30 – April 4 2008.

NEW DISCOVERIES, INVENTIONS, PATENT DISCLOSURES

U.S. Provisional Patent Applicaton No. 60/938,858
Inventors: Roberto Merlin and Anthony Grbic
Title: Apparatus for Sub-wavelength Near-field Focusing of Electromagnetic Waves
Filed: May 18, 2007
Assignee: Regents of the University of Michigan, Office of Technology Transfer, Wolverine Tower, Room 2071, South State Street, Ann Arbor, MI, 48109-1280.

HONORS / AWARDS

NSF Faculty Early Career Development Award (ECCS-0747623)

Air Force Office of Scientific Research Young Investigator Award (FA9550-08-1-0067),

REFERENCES

[1] A. Grbic, "A 2-D Composite Medium Exhibiting Broadband Negative Permittivity and Permeability," in *IEEE Antennas and Propagation Society International Symposium*, pp. 4133-4136, Albuquerque, NM, July 9-14 2006.

[2] S. M. Rudolph and A. Grbic, "A Volumetric Negative- Refractive-Index Medium Exhibiting Broadband Negative Permeability," *Journal of Applied Physics*, **102**, 013904, July 2007.

[3] S. M. Rudolph and A. Grbic, "A Printed Circuit Implementation of a Broadband Volumetric Negative-Refractive-Index Medium," *IEEE Antennas and Propagation Society International Symposium*, pp. 2542-2545, Honolulu, HI, June 9-15 2007.

[4] S.M. Rudolph, A. Grbic, "Super-Resolution Focusing Using Broadband, Volumetric NRI Media," *IEEE Trans. on Antennas and Propagation*, under review, submitted July 2007.

[5] S.M. Rudolph, A. Grbic, "Modeling of Volumetric Negative-Refractive-Index Media Using Multiconductor Transmission-Line Analysis, *Applied Computational Electromagnetics Society Conference (ACES)*, 4 pages, Niagara Falls Canada, March 30 – April 4 2008.

[6] A. F. Starr, P.M. Rye, D.R. Smith and S. Nemat-Nasser, "Fabrication and Characterization of a Negative-Refractive-Index Composite Metamaterial," *Physical Review B*, **70**, 113102, September 2004.

[7] B.I. Popa, S.A. Cummer, "Determining the Effective Electromagnetic Properties of Negative-Refractive-Index Metamaterials Parameters from Internal Fields," *Physical Review B*, **72**, 165102, October 2005.

[8] D.R. Smith, D. Schurig, R. Rosenbluth, S. Schultz, S.A. Ramakrishna, and J.B. Pendry, Limitations on Subdiffraction Imaging with a Negative Refractive Index Slab," *Applied Physics Letters*, **82**, pp. 1506-1508, March 2003

[9] A. Grbic and G. V. Eleftheriades, Practical Limitations of Subwavelength Resolution Using Negative-Refractive-Index Transmission-Line Lenses," *IEEE Transactions on Antennas and Propagation*, **53**, pp. 3201-3209, October 2005.

[10] R. Merlin, "Analytical Solution of the Almost-Perfect-Lens Problem," *Applied Physics Letters*, **84**, pp. 1290-1292, February 2003.

[11] J. Pendry, A. J. Holden, D. J. Robbins and W. J. Stewart, "Magnetism from Conductors and Enhanced Nonlinear Phenomena", *IEEE Transactions on Microwave* Theory and Techniques, 47, pp. 2075 – 2084, Nov. 1999

[12] V. M. Shalaev, "Optical Negative-Index Metamaterial," Nature Photonics, **1**, pp. 41-48, January 2007.

[13] C. G. Parazzoli, R. B. Greegor, J. A. Nielsen, M. A. Thompson, K. Li, A. M. Vetter, M. H. Tanielian and D. C. Vier, "Performance of a Negative Index of Refraction Lens", *Applied Physics Letters*, **84**, pp. 3232 – 3234, April 2004.

[14] K. Aydin, I. Bulu, and E. Ozbay, "Subwavelength Resolution with a Negative-Index Metamaterial Superlens", *Applied Physics Letters*, **90**, 214502, June 2007.

[15] A. Grbic, G.V. Eleftheriades, "Overcoming the Diffraction Limit with a Planar Left-Handed Transmission-Line Lens," *Physical Review Letters*, **92**, 117403, March 2004.

[15] D. Schurig, D.R. Smith, "Negative Index Lens Aberrations," *Physical Review E*, **70**, 065601, December 2004.

[16] A. Grbic, G.V. Eleftheriades, "Overcoming the Diffraction Limit with a Planar Left-Handed Transmission-Line Lens," *Physical Review Letters*, **92**, 117403, March 2004.

[17] D. Schurig, D.R. Smith, "Negative Index Lens Aberrations," *Physical Review E*, **70**, 065601, December 2004.

[18] A. Grbic, G.V. Eleftheriades, " Experimental Verification of Backward-Wave Radiation From a Negative Refractive Index Metamaterial," *Journal of Applied Physics*, **92**, pp. 5930-5935, November 15, 2002.

[19] M. Tabib-Azar, M. Katz, J.L. LeClair, "Evanescent Microwaves: a Novel Super-Resolution Noncontact Nondestructive Imaging Technique for Biological Applications," *IEEE Trans. on Instrumentation and Measurement*, **48**, pp. 1111-1116, December 1999.

APPENDIX

S.M. Rudolph, A. Grbic, “Super-Resolution Focusing Using Broadband, Volumetric NRI Media,” *IEEE Trans. on Antennas and Propagation*, under review, submitted July 2007.

Super-Resolution Focusing using Volumetric, Broadband NRI Media

S. M. Rudolph, Student Member, IEEE and Anthony Grbic, Member, IEEE

Abstract— **In this paper, we describe the design, fabrication and testing of broadband negative permeability and broadband negative-refractive-index (NRI) metamaterials. The metamaterials are designed to address two major limitations of current NRI media: high loss and narrow bandwidth of operation. The proposed NRI design has a backward-wave bandwidth of 44.3%. This large bandwidth allows the structure to operate away from resonances, where the loss is significantly lower. The stopband characteristics of a $\lambda_0/3$ slab of negative permeability medium were measured. In addition, the focusing characteristics of the NRI medium were also tested and resolution beyond the diffraction limit was experimentally observed. The slab measured in this paper produced a resolution enhancement of 2.0 over a bandwidth of 0.33%.**

I. Introduction

In 1968, Victor Veselago theoretically showed that a flat slab of material exhibiting both negative permittivity and negative permeability would act as an unusual lens and focus electromagnetic waves [1]. Nearly forty years later, John Pendry revealed that Veselago's lens could also resonantly amplify the evanescent waves that decay away from a source, thus allowing them to contribute to the image at the focal plane [2]. In this way, the image of the source could be reconstructed with resolution beyond the diffraction limit. NRI materials were experimentally verified shortly thereafter, providing the first step toward making such lenses a reality [3].

In 2004, super-resolution was experimentally verified using a planar negative-refractive-index (NRI) transmission-line lens [4]. Super-resolution at ultraviolet and infrared frequencies was subsequently achieved by means of focusing the evanescent spectrum using silver and silicon carbide negative permittivity slabs, respectively [5–7]. Focusing using volumetric NRI media at microwave frequencies was also demonstrated [8, 9], but these NRI lenses could not recover the evanescent spectrum in order to overcome the diffraction limit. The degraded performance of these lenses was attributed to high conductor losses and impedance or refractive index mismatches.

In this paper, resolution beyond the diffraction limit is demonstrated experimentally using a volumetric NRI lens. The lens is based on a structure exhibiting a broadband negative index of refraction, which was proposed in [10] and subsequently analyzed in [11]. In [11], the structure was shown to exhibit low-loss characteristics at its operating frequency, making this structure well-suited for the design of a NRI microwave superlens. A NRI structure that could be manufactured using printed circuit board (PCB) technology was presented in [12]. A slightly modified version of this structure, shown in Figure 1, was used in the experiments described in this paper. The design and fabrication, which were critical to the success of this lens, are described in detail.

The authors are with the Radiation Laboratory, Department of Electrical Engineering and Computer Science, University of Michigan, Ann Arbor. E-mails: scotmich@umich.edu, agrbic@umich.edu

II. Design of the Broadband NRI Lens

Only a lossless lens with homogeneous and isotropic relative permeability, μ_r, and permittivity, ϵ_r, equal to the negative of those in the surrounding medium can give rise to perfect imaging [2]. In order to achieve sub-wavelength focusing in free-space, the NRI medium must have minimal loss and an ϵ_r and μ_r very close to -1. As mentioned in the introduction, impedance mismatches and high loss prevented previous volumetric NRI lenses from achieving super resolution [13–16]. These issues are addressed in the proposed structure that was used to demonstrate super resolution.

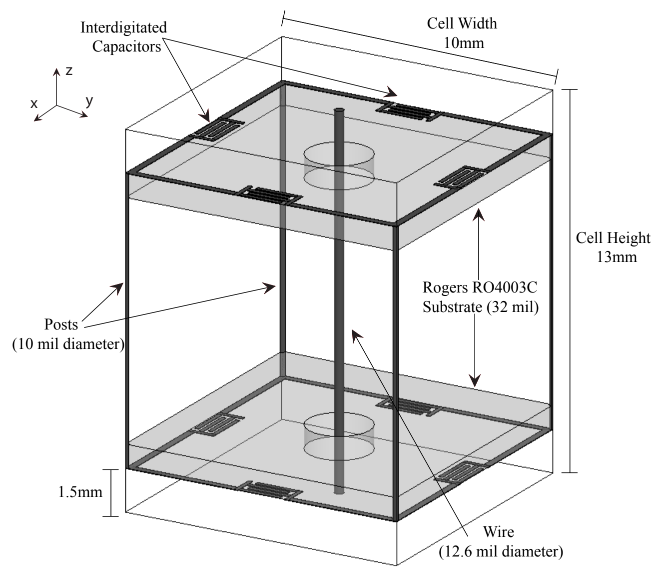

Fig. 1. Final design of the NRI unit cell. The structure exhibits two-dimensional, isotropic impedance and propagation characteristics.

The structure presented in [12] is shown in Figure 2. This cell was found to exhibit slight asymmetry in the $\vec{x}$ direction, since the vertical strip was printed on only one side of the substrate. The Bloch impedance was different for propagation in the negative and positive $\vec{x}$ directions, resulting in an impedance mismatch at both interfaces of the lens. This asymmetry was remedied by replacing the PCB strip with a wire, the diameter of which could be varied to adjust its inductance, and thus change the permittivity

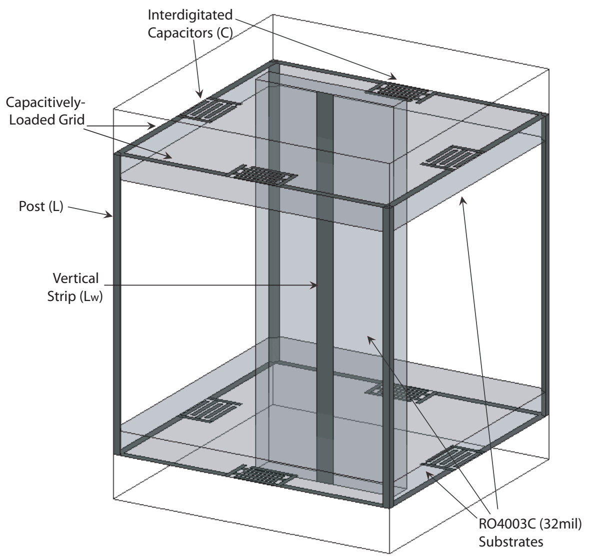

Fig. 2. Initial design of the NRI unit cell. The asymmetry found in this design caused an impedance mismatch in the $\vec{x}$ direction.

of the medium, as shown in Figure 1. A four-cell slab of this structure was designed to have effective material parameters of $\epsilon_r = -1$ and $\mu_r = -1$ at the design frequency of 2.45GHz. The simulated scattering parameters of this four-cell slab were obtained using Ansoft's HFSS. All simulations were performed with conductors as the boundaries on the top and bottom of the unit cell. This ensured that the electric field was always polarized in $\vec{z}$ direction and more accurately represented the experiments described in section IV.

The effective material parameters were designed to be $\epsilon_r = -1.00$ and $\mu_r = -1.01$ at 2.45GHz for the lossless structure in Figure 1. When the substrate and conductor losses were added to the simulation, the effective material parameters changed to $\epsilon_r = -0.99 + j0.011$ and $\mu_r = -1.02 - j0.054$. Equivalently, the refractive index and wave impedance became $n = -1.01 - j0.021$ and $\eta_{Bloch} = 384 + j12\Omega$, which is well-matched to the free-space wave impedance of 377Ω. For a time-harmonic progression of $e^{j\omega t}$, the imaginary part of the index of refraction should be negative in passive media, as calculated above. This may make the positive imaginary part of ϵ_r appear unphysical, however it is actually expected. This effect has been documented in other split-ring resonator or NRI structures [17] and is attributed to an antiresonance in permittivity in response to the permeability resonance. In Figure 3, the power loss in the proposed structure is confirmed to be positive for all frequencies.

The simulated value for n gave an attenuation constant of $\alpha = 1.08$Np/m and a propagation constant of $\beta = 51.6$rad/m at 2.45GHz. A common means of quantifying the loss in NRI media is to use the figure of merit (FOM) [18, 19], which is defined as

$$FOM = |\frac{n'}{n''}| \tag{1}$$

where n' and n'' are the real and imaginary parts of the refractive index, respectively. Using this equation, the figure of merit for this structure was calculated to be $FOM = 47.9$ at the design frequency. The planar NRI transmission line (TL) used to verify super resolution in [4] had a figure of merit of $FOM = 32.14$. The figure of merit of the proposed NRI medium is better than that observed in the NRI TL predominantly because the wire used to achieve negative permittivity in the proposed NRI medium has a higher Q than the lumped element inductors used in the NRI TL.

The dispersion curve of the proposed NRI structure, which is plotted in Figure 4, indicates that it exhibits a backward-wave bandwidth of 44.3%, ranging from 1.83GHz to 2.86GHz. Due to the broadband nature of the NRI region, the operating frequency is no longer close to the resonant frequency at which permeability changes from highly-positive to highly-negative values, as is the case for the SRR/wire medium. The losses are lower the further the operating frequency is from this resonance [20]. This fact is clearly displayed in Figure 3, which shows the material losses of a four-cell slab as a function of frequency. The power lost due to conductor and dielectric losses was 0.37dB at 2.45GHz for four cells or 0.092dB/cell (equivalently 0.092dB/cm), demonstrating that this NRI structure has minimal power loss at the operating frequency.

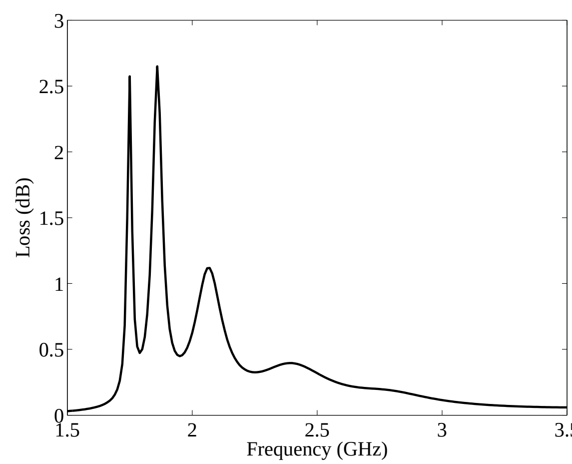

Fig. 3. Simulated conductor and dielectric losses for a four-cell slab given by $Loss(dB) = -20\log\left(\sqrt{|S_{11}|^2 + |S_{21}|^2}\right)$. The four peaks in loss occur when the four-cell slab is at resonant lengths of 180°, 360°, 540° and 720°.

III. Fabrication

First, a negative permeability medium was fabricated by printing a capacitively-loaded grid onto two 32 mil RO4003 substrates ($\epsilon_r = 3.38$), as shown in Figure 5. The unit cell size of the grid was 1cm in both the $\vec{x}$ and $\vec{y}$ directions. The capacitors were interdigitated, printed capacitors optimized through simulation to have a value of 322fF. Small holes were drilled at the junctions of the grid to accommodate the posts. The two PCBs were then spaced 1cm apart and the posts, made from 30AWG (10 mil diameter) copper wire, were soldered between the two. The holes at the grid-junctions were plated with copper to ensure good electrical

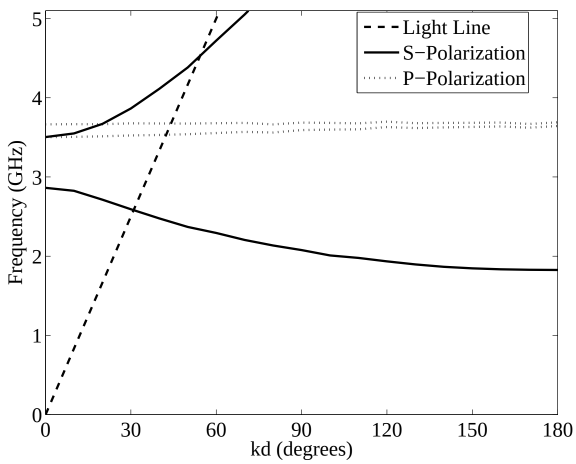

Fig. 4. Simulated dispersion curve of the infinite NRI medium.

connection between the posts and the capacitively-loaded grid. The negative permeability slab was four cells thick ($\vec{x}$ direction) and had a width of 15 cells ($\vec{y}$ direction). To emulate infinite periodicity in the vertical ($\vec{z}$) direction, the slab was placed in between two parallel plates, spaced 1.3cm apart. Foam blocks were cut to support the structure, ensuring a 1.5mm separation was maintained between the plates and the capacitively-loaded grid.

Once the negative permeability medium was fabricated, making a NRI medium was only a matter of adding wires to achieve negative permittivity. The holes in the center of the negative permeability unit cell (2.25mm in diameter) were drilled to allow these wires to pass through. These holes are depicted in the unit cell enlargment in Figure 5. Copper-plated RO4003 substrates were used as the parallel plates. Copper-plated holes were machined into these ground planes to allow for proper grounding of the negative permittivity wires. The wires were 28AWG (12.6 mil diameter) and 1.3cm in length. They were soldered between the top and bottom parallel plates to create the NRI lens, also four cells thick with a width of 15 cells, which is shown in Figure 6.

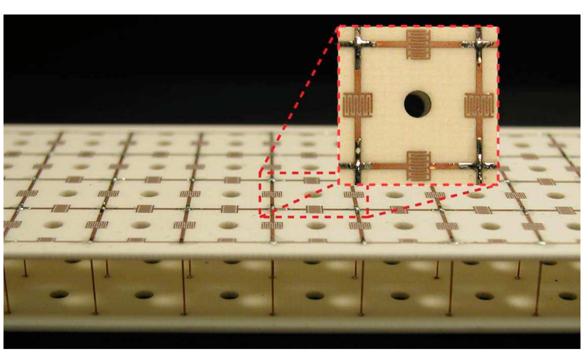

Fig. 5. Picture of the negative permeability slab with an enlargement of a grid unit cell.

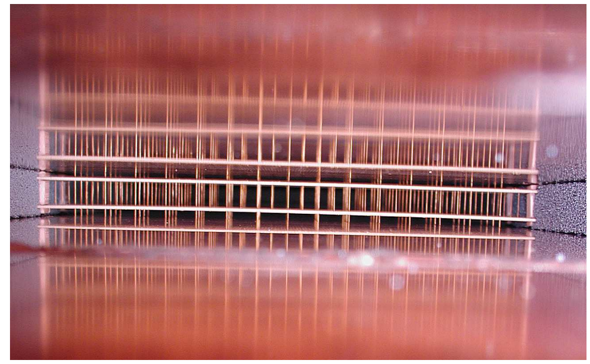

Fig. 6. Picture of the NRI lens within the parallel-plate waveguide. Images of the NRI slab can be seen in the photograph.

IV. Experiments

All the experiments for the negative permeability and NRI media were conducted in a parallel-plate waveguide (PPW) environment. Gradient absorber FL-4500CL, manufactured by ETS-Lindgren, was used to prevent reflection at the edge of the PPW, similar to that described in [21]. While Justice et. al. used wedge-shaped absorber, the resonant frequency of 1.82GHz and the size of the plates (18-by-24 inches) did not permit wedges of sufficient size to fully attenuate the low frequency radiation. Nevertheless, tests confirmed that the gradient absorber successfully eliminated the reflections from the edges of the PPW. The absorber was cut into 1.3cm slabs (to ensure the correct unit cell height) and arranged in a rectangle around the lens as shown in Figure 7. Also pictured in Figure 7 are the Amphenol Connex 132147 coaxial connectors, which were used as probes to provide the fixed-point excitations inside the PPW. The dielectric jackets covering the connectors were trimmed such that only the center conductor protruded from the surface of the plates.

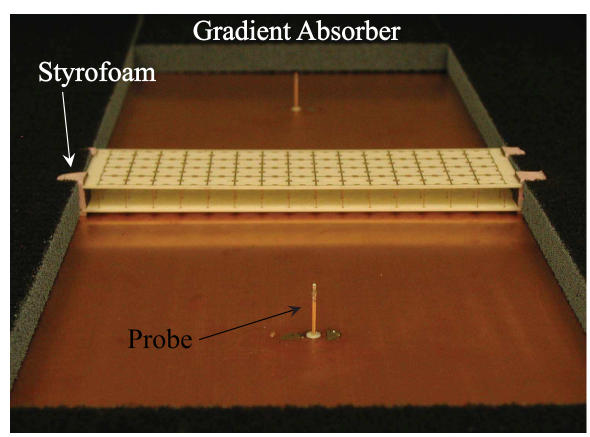

Fig. 7. Photograph of the bottom plate of the parallel-plate waveguide with gradient absorber walls and the negative permeability slab. This shows the two-probe experimental setup to measure the stopband characteristics of the negative permeability medium. The probes have been placed 7cm from the cell so that only the transmission of the propagating waves is considered.

A. Negative Permeability Stopband Measurements

When the permeability and permittivity of a medium have opposite signs, waves naturally attenuate. The negative permeability medium, therefore, exhibits a stopband over the region where negative permeability occurs. This region is shown by the dispersion curve of the negative permeability region in Figure 8. The negative permeability medium was tested to verify its attenuation characteristics. This was done by placing two sources (coaxial connector probes) 7cm away from either face of the slab (see Figure 7). The air/lens interfaces were consequently beyond the reactive near-field of the probes. This ensured that all of the evanescent fields emanating from the probes would attenuate sufficiently before reaching the slab, eliminating the possibility of evanescent field recovery. This was important for stopband measurements because any evanescent waves that reached the first lens interface could be resonantly amplified, producing higher-than-expected fields at the source. Further, because the distance from the source to the slab was greater than the thickness of the slab, no internal nor external focusing of the evanescent spectrum could occur. The results of these experiments are displayed in Figure 9. The plot shows a total attenuation of better than 20dB for the four-cell slab with respect to the parallel plate environment without the slab present. At the design frequency of 2.45GHz, the slab corresponds to an electrical thickness of just less than $\frac{\lambda_0}{3}$. Therefore, the negative permeability slab acts as a highly-attenuating stopband medium.

The exact frequencies over which the medium exhibits a stopband (a negative permeability) cannot be accurately determined from Figure 9, since the impedance, index of refraction and attenuation constant of the slab all play an important role in determining the magnitude of S_{21}. In contrast, the stopband edges are clearly defined in Figure 8, which shows the propagating eigenmodes of the negative permeability medium. This is because the eigenmode analysis assumes infinite periodicity, and, therefore, even the slightest attenuation constant results in a stopband. In a finite structure, such as the one shown in Figure 5, the small attenuation constants near the stopband edges do not significantly affect the transmission through the slab. Therefore, one cannot say with exact certainty where the stopband begins and ends based only on the transmission data.

Similar to arrays of split-ring resonators, the broadband negative permeability slab exhibits a high, positive permeability at frequencies below the low-frequency stopband edge. In this same frequency range, the electrical loading caused by the slab also increases the permittivity. Together, these two effects increase the positive index of refraction of the medium while maintaining a wave impedance that is similar to that of free space. Consequently, the slab remains reasonably well-matched to free space and refracts the cylindrical wave emanating from the transmitting probe toward the slab's normal, increasing the signal received at the receiving probe. This explains why both the measured and simulated magnitudes of S_{21} are greater with the slab than without it, at frequencies below the stopband.

At the frequencies above the high-frequency edge of the stopband, the magnitude of S_{21} remains low due to the reflections from the slab. As the permeability transitions from negative to positive, it remains much lower than that of free space. Since the permittivity of the medium is still high due to the electrical loading caused by the slab, the slab exhibits a low impedance and reflects much of the power incident on it. This results in low transmission even at frequencies above the high-frequency edge of the stopband. For these reasons, the eigenmode analysis shown in Figure 8 is typically used to determine where the medium exhibits a stopband due to negative permeability rather than transmission data.

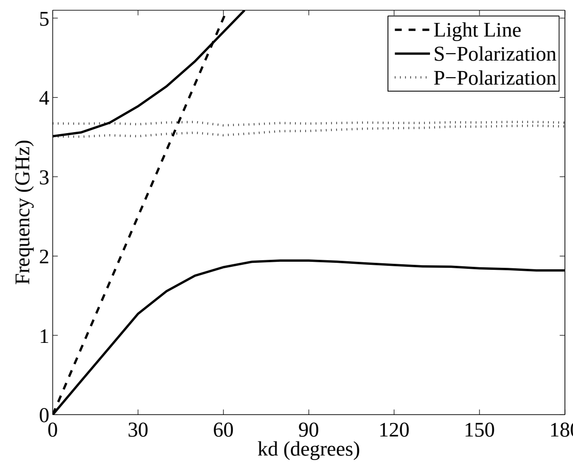

Fig. 8. Simulated dispersion curve of the infinite negative permeability medium.

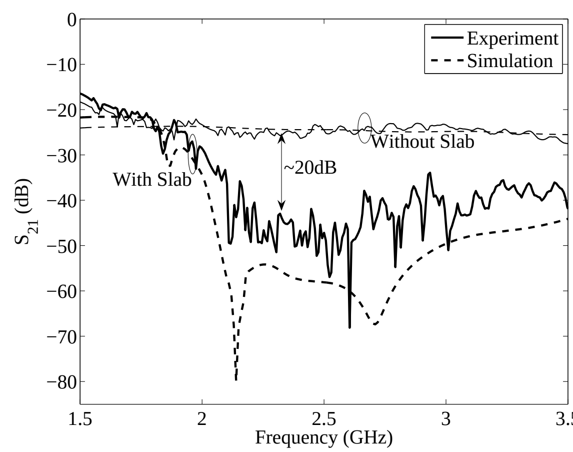

Fig. 9. Stopband performance of the negative permeability slab shown in Figure 5. Measurements are denoted by the solid line and simulated results are shown with the dashed line. The darker lines indicate that the slab is present, while the lighter lines indicate that the slab is removed.

B. Negative-Refractive-Index Focusing Measurements

To test the focusing characteristics of the NRI medium, the source was moved to a location 2cm away from the first interface of the lens. Now a substantial portion of the evanescent spectrum could reach the lens before decaying below the noise floor and could therefore be recovered by the NRI lens. In order to measure the fields over a two-dimensional space within the PPW containing the NRI lens, a small slit less than 3mm in height was cut into the absorber at the end of the PPW opposite the source. A horizontal probe made out of 0.086in semirigid cable, with the inner conductor polarized in the vertical direction, was inserted into the slit and could be moved independently with respect to the PPW. The probe was then used to scan the electric fields at the exit face of the lens and beyond using an automated computer routine that controlled the position of the translation stage to which the probe was attached. This program also interfaced with a HP8753D network analyzer to store the S-parameters observed at the current probe location. This procedure is diagramed in Figure 10. The performance of the probe was tested by measuring the fields within the empty PPW, that is, without the NRI lens present. The fields of the PPW were not disturbed by the presence of the probe in any visible way (see Figure 9).

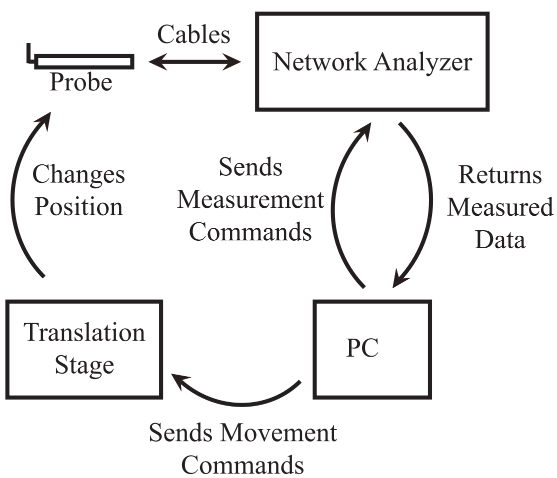

Fig. 10. Block diagram of the experimental setup.

The NRI lens performed best at 2.424GHz, which corresponds to a shift of 1% from the design frequency of 2.45GHz. Since this frequency was found to be optimal for two separate lenses that were made, the shift can primarily be attributed to the manufacturing tolerances in the fabrication of the interdigitated capacitors. Figure 11 shows contour plots of both phase and magnitude of a region up to 6.5cm beyond the second interface of the lens. Measurements were taken every 1.2mm in the $\vec{x}$ (longitudinal) direction and every 2.5mm in the $\vec{y}$ (transverse) direction. To prevent the wires from being damaged by the probe or vice versa, the scan was started 2mm away from the face of the lens. The high fields observed close to the interface of the lens in Figure 11(a) indicate the resonant amplification of the evanescent spectrum. The phase diagram shows a cylindrical wave emanating from the focus (located at [x,y] = [2,0]), confirming source reconstruction.

Figure 12 plots the normalized measured electric field amplitude along the image plane (x = 2cm) as well as the diffraction-limited curve as a reference. The diffraction-limited curve is given by the following equation [4]:

$$
\begin{aligned}
&C\int_{\infty}^{\infty}\frac{e^{-jk_{x1}d}e^{-jk_{x2}d}e^{-jk_y y}}{k_{x1}}dk_y \\
&k_{x1}=-k_{x2}=\sqrt{k_0^2-k_y^2}\text{ for }k_y<k_0, \\
&k_{x1}=k_{x2}=-j\sqrt{k_y^2-k_0^2}\text{ for }k_y>k_0
\end{aligned}
\tag{2}
$$

where d = 4cm is defined as the thickness of the lens, k_{x1} represents the $\vec{x}$ directed propagation outside of the lens, k_{x2} represents the $\vec{x}$ directed propagation inside of the lens, and C is a normalization constant [4]. This equation accounts for both the propagating and evanescent portions of the spectrum at the focal plane. The propagating spectrum experiences phase advancement in the longitudinal direction as it travels through the NRI slab, hence $k_{x1}=-k_{x2}$ for $k_y<k_0$. The evanescent waves, on the other hand,are assumed to decay in both media, thus producing a diffraction-limited curve. It is apparent by comparing the diffraction-limited curve and the experimental data that the proposed lens design does achieve super-resolution. The half-power beamwidth of the diffraction-limited curve is 0.36λ, as is expected for a line source of TM polarization outside of the reactive near field. The half-power beamwidth of the experimental curve is 0.252λ, which corresponds to a resolution enhancement of 2.0. In the experiment, this resolution enhancement is maintained over a bandwidth of 8MHz or 0.33%.

The bandwidth of resolution enhancement is notably smaller than the backward-wave bandwidth, but this is inherent to the phenomenon of super resolution. As mentioned previously and rigorously shown in [13–16], to achieve super resolution at the image plane, μ_r and ϵ_r must be very close to -1. Because backward waves are inherently dispersive, the material parameters necessarily diverge from the ideal values as frequency changes. The resolution enhancement bandwidth measures the bandwidth over which the material parameters are close enough to produce a resolution enhancement of a particular value, in this case R_e = 2.0. This frequency range can be only a fraction of the full backward-wave bandwidth.

The resolution enhancement is given by the equation

$$R_e=\frac{k_{ymax}}{k_0} \tag{3}$$

where k_{ymax} is the maximum transverse wavenumber that contributes to the image. This quantity can be obtained by finding k_{xmax}, which is given by the equation

$$k_{xmax}=\frac{-j\ln|\Gamma_1|}{d}=\frac{-j}{d}\ln\left|\frac{\frac{\omega\mu_n}{k_{xn}}-\frac{\omega\mu_0}{k_{x0}}}{\frac{\omega\mu_0}{k_{x0}}+\frac{\omega\mu_n}{k_{xn}}}\right| \tag{4}$$

where Γ_1 is the Fresnel reflection coefficient at the first interface of the lens, k_{xn} is the magnitude of the $\vec{x}$ component of the wave vector in the NRI lens, μ_n is the permeability

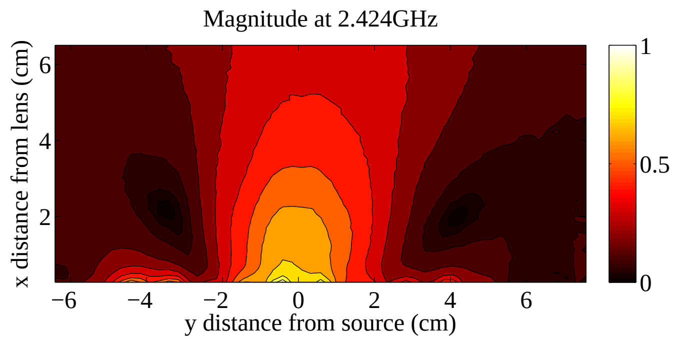

(a)Contour plots of the normalized measured electric field magnitude on the exit side of the NRI lens

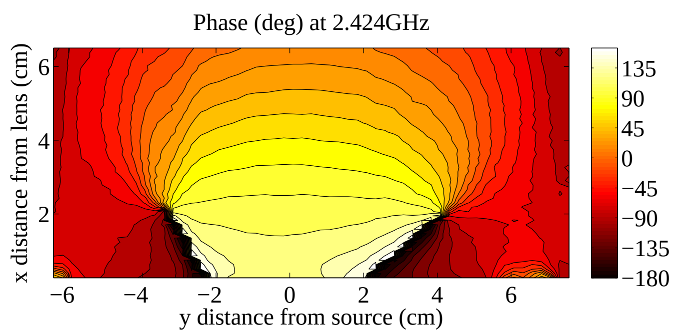

(b)Contour Plots of the Measured Unwrapped Electric Field Phase on the exit side of the NRI lens

Fig. 11. Plots of the measured vertically-polarized electric field at 2.424GHz

in the NRI lens and d is again the lens thickness. The indices of refraction for the lens and free-space are predicted to be approximately the same, therefore $k_{xn} \approx k_{x0}$. The equation simplifies to

$$k_{xmax} \approx \frac{-j}{d} \ln \left| \frac{\mu_r - 1}{\mu_r + 1} \right| \tag{5}$$

where μ_r is relative permeability of the NRI lens as given in the second section of this paper. Once k_{xmax} is found, k_{ymax} is given by the separation relation. Then using Equation (3), the resolution enhancement was calculated to be 2.01, which is in excellent agreement with the experimental value of 2.0.

Alternatively, the expected resolution enhancement can be found by deriving a transfer function for an isotropic, homogeneous NRI lens of thickness d, infinite width and the same material parameters that were reported in section II. This method accounts for reflections at the interface due to impedance mismatch and losses within the slab. From this transfer function, the resolution enhancement was determined to be 1.98, again in good agreement with the experiments.

Both of the previous methods used to calculate the resolution enhancement assume that the slab is infinite in extent. To verify that these equations are still applicable to the finite structure used in the experiments, two homogeneous slabs having the same material parameters as those given in section II were simulated using HFSS. The first had

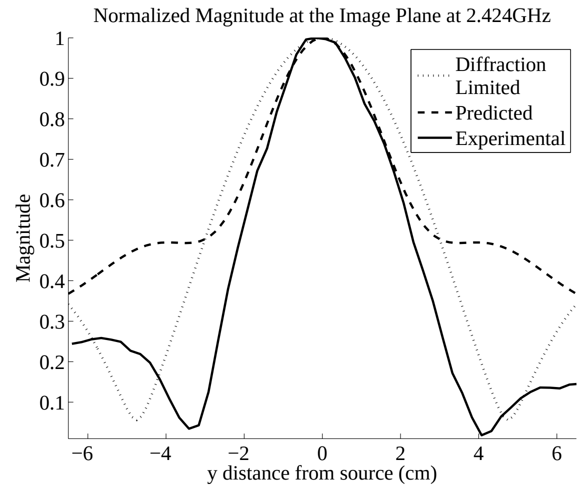

Fig. 12. Normalized electric field magnitude at the image plane (x = 2cm). The experimental field magnitude is plotted with a solid line, the theoretical diffraction-limited field magnitude is plotted with a dotted line and the field magnitude as predicted by assuming a homogeneous, isotropic, lossy slab of the simulated material parameters given in the second section is plotted with a dashed line.

a transverse ($\vec{y}$) dimension equal to 15cm; the second had a transverse dimension equal to 40cm. These widths correspond to numerical apertures of $NA = sin(75.1°) = 0.966$ and $NA = sin(84.3°) = 0.995$, respectively. The normalized electric field magnitude at the image plane is shown in Figure 13. The smaller numerical aperture exhibited a resolution of 0.248λ and the larger numerical aperture exhibited a resolution of 0.255λ, which both match the measured value of 0.252λ. This shows that the resolution enhancement is not significantly affected by the truncation of the structure.

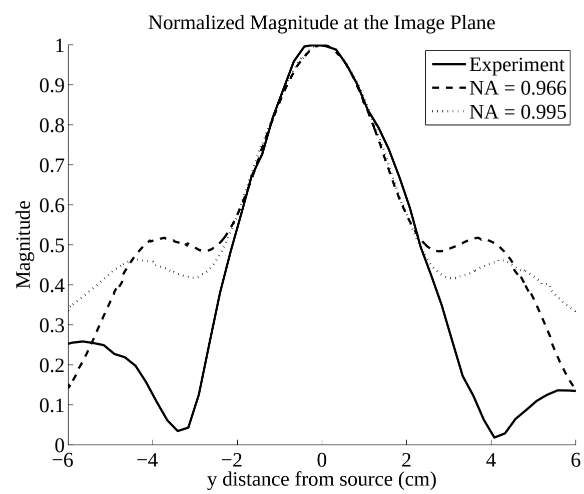

Fig. 13. Normalized electric field magnitude at the image plane (x = 2cm) for two homogeneous slabs having numerical apertures of 0.966 (dashed) and 0.995 (dotted) compared to the experimental results (solid).

V. Conclusion

In this paper, we experimentally verified super-resolution using a volumetric NRI lens design. The simulation and experiment both produced resolution enhancements of 2.0. This was accomplished using a flat slab of a broadband NRI medium, which owes its increased bandwidth to an extended negative permeability region. The structure was also shown to have low-loss characteristics at the operating frequencies, which aided in the amplification of the evanescent spectrum. The stopband characteristics of the broadband negative permeability structure were also measured and shown to produce 25dB of attenuation for the four-cell slab.

VI. Acknowledgements

This work was supported by the Air Force Office of Scientific Research under grant number FA9550-07-1-0029.

The authors would like to thank Carl Pfeiffer for his assistance in the measurements and the processing of the experimental data, as well as Saturn Electronics Corp. for the fabrication of the printed circuit boards.

References

[1] V.G. Veselago, "The Electrodynamics of Substances with Simultaneously Negative Values of ϵ and μ," *Sov. Phys. Usp.*, vol. 10, pp. 509–514, Jan-Feb 1968.

[2] J.B. Pendry, "Negative Refraction Makes a Perfect Lens," *Physical Review Letters*, vol. 85, pp. 3966–3969, October 2000.

[3] R.A. Shelby, D.R. Smith, and S. Schultz, "Experimental Verification of a Negative Index of Refraction," *Science*, vol. 292, pp. 77–79, April 2001.

[4] A. Grbic and G.V. Eleftheriades, "Overcoming the Diffraction Limit with a Planar Left-Handed Transmission-Line Lens," *Physical Review Letters*, vol. 92, no. 11, pp. 117403, March 2004.

[5] N. Fang, H. Lee, C. Sun, and X. Zhang, "Sub-Diffraction Limited Optical Imaging with a Silver Superlens," *Science*, vol. 308, pp. 534–537, April 2005.

[6] D. O. S. Melville and R. J. Blaikie, "Super-Resolution Imaging through a Planar Silver Slab," *Optics Express*, vol. 13, no. 6, pp. 2127–2134, March 2005.

[7] T. Taubner, D. Korobkin, Y. Urzhumov, G. Shvets, and R. Hillenbrand, "Near-Field Microscopy Through a SiC Superlens," *Science*, vol. 313, pp. 1595, September 2006.

[8] A. A. Houck, J. B. Brock, and I. L. Chuang, "Experimental Observations of a Left-Handed Material That Obeys Snell's Law," *Physical Review Letters*, vol. 90, no. 13, pp. 137401, April 2003.

[9] C. G. Parazzoli, R. B. Greegor, J. A. Nielsen, M. A. Thompson, K. Li, A. M. Vetter, and D. C. Vier, "Performance of a Negative Index of Refraction Lens," *Applied Physics Letters*, vol. 84, no. 17, pp. 3232–3234, April 2004.

[10] A. Grbic, "A 2-D Composite Medium Exhibiting Broadband Negative Permittivity and Permeability," in *IEEE Antennas and Propagation Society International Symposium*, Albuquerque, NM, July 9-14 2006, pp. 4133–4136.

[11] S. M. Rudolph and A. Grbic, "A Volumetric Negative-Refractive-Index Medium Exhibiting Broadband Negative Permeability," *Journal of Applied Physics*, vol. 102, July 2007.

[12] S. M. Rudolph and A. Grbic, "A Printed Circuit Implementation of a Broadband Volumetric Negative-Refractive-Index Medium," in *IEEE Antennas and Propagation Society International Symposium*, Honolulu, HI, June 10-15 2007, pp. 1067–1070.

[13] D.R. Smith, D. Schurig, R. Rosenbluth, S. Schultz, S.A. Ramakrishna, and J.B. Pendry, "Limitations on Subdiffraction Imaging with a Negative Refractive Index Slab," *Applied Physics Letters*, vol. 82, pp. 1506–1508, March 2003.

[14] A. Grbic and G. V. Eleftheriades, "Practical Limitations of Subwavelength Resolution Using Negative-Refractive-Index Transmission-Line Lenses," *IEEE Transactions on Antennas and Propagation*, vol. 53, no. 10, pp. 3201–3209, October 2005.

[15] R. Merlin, "Analytical Solution of the Almost-Perfect-Lens Problem," *Applied Physics Letters*, vol. 84, no. 8, pp. 1290–1292, February 2003.

[16] V. Podolskiy and E. Narimanov, "Near-sighted superlens," *Optics Letters*, vol. 30, no. 1, pp. 75–77, January 2005.

[17] T. Koschny, P. Markǒs, D. R. Smith, and C. M. Soukoulis, "Resonant and antiresonant frequency dependence of the effective parameters of metamaterials," *Phys. Rev. E*, vol. 68, pp. 065602–065605, 2003.

[18] C. M. Soukoulis, S. Linden, and M. Wegener, "Negative Refractive Index at Optical Wavelengths," .

[19] V. M. Shalaev, "Optical Negative-Index Metamaterial," *Nature Photonics*, vol. 1, pp. 41–48, January 2007.

[20] J. B. Pendry, A. J. Holden, D. J. Robbins, and W. J. Stewart, "Magnetism from Conductors and Enhanced Nonlinear Phenomena," *IEEE Transactions on Microwave Theory and Techniques*, vol. 47, pp. 2075–2084, November 1999.

[21] B. J. Justice, J.J. Mock, L. Guo, A. Degiron, D. Schurig, and D.R. Smith, "Spatial Mapping of the Internal and External Electromagnetic Fields of Negative Index Metamaterials," *Optics Epress*, vol. 14, no. 19, pp. 8694–8705, September 2006.